Volume 19, Number 1, 2026. pp. 65-74

Jordan Journal of Physics

ARTICLE

Structural and Optical Properties of Calcium-doped Zinc Oxide Thin Film Deposited by the PLD Method

I. H. Mejri[a], **J. P. B. Silva**[b], **M. Nouiri**[a], **A. Bouloufa**[c], **Z. Ben Ayadi**[a] and **L. El Mir**[a]

[a] *Laboratory of Physics of Materials and Nanomaterials Applied at Environment, Faculty of Sciences of Gabes, University of Gabes, LR05ES14, 6072, Gabes, Tunisia.*

[b] *Centre of Physics of University of Minho (CF-UM), Campus de Gualtar, 4710-057 Braga, Portugal.*

[c] *Laboratoire d'Electrochimie et Matériaux, Université Ferhat Abbas Sétif-1, Algeria.*

DOI: **https://doi.org/10.47011/19.1.7**

Received on: 05/11/2024; *Accepted on: 28/01/2025*

Abstract: A sample of calcium-doped zinc oxide (CZO) thin films of varying thicknesses were prepared by the pulsed laser deposition technique (PLD) on glass substrates. The film samples were grown at constant oxygen pressure. The pulsed laser deposition target used was Ca-doped zinc oxide 3 at. % nanopowder synthesised by a modified sol-gel process. The structural, morphological and optical properties of the CZO thin film were studied. From the X-ray diffraction analysis, the orientation of Ca-doped zinc oxide thin films was found to be along the c-axis, displaying only a (002) diffraction peak. The X-ray diffraction spectra revealed that the crystalline quality of the film was enhanced and grain size grew by increasing the film thickness. Cross-sectional microscopy images show the formation of columnar structure in the obtained thin film with low surface roughness when the film thickness increases. CZO thin film is highly transparent in the visible wavelength region with a transmittance higher than 90% for the lowest thickness. The calculated optical band gap is approximately 3.4 eV. The obtained results revealed that our samples are promising as transparent conducting oxide layers in many technological applications.

Keywords: Ca-doped ZnO nanoparticles, Sol-gel, PLD, Thin films, Optical properties.

1. Introduction

Recently, transparent conducting zinc oxide (ZnO) thin film has been investigated as an important semiconductor in many fields. Indeed, the interesting optical and electrical properties of these materials can make them potential candidates for various applications [1-6]. Among these properties, the high transparency in the visible region, the wide band gap, the high natural abundance, and the chemical stability can be observed. Thus, the ZnO material can be used as a transparent electrode in solar cells, light-emitting diodes (LED), photocatalytic support, thin film transistors, UV photodetector and various optoelectronic devices [7-14]. Therefore, to serve and improve these applications, many researchers used different doping elements to control and optimize the physical properties of ZnO. For example, some metals of the Group III elements, such as (Al, In), have been used to improve the conductivity and control the electrical properties of ZnO [15]. For the photoluminescence properties, noble metals such as gold have been used as doping elements [16]. Also, for their magnetic properties, elements such as (Fe, Mn, Co and Cr) serve well as transition metals [17, 18]. The elements of group I (Li, Na) have been used to realize a p-type semiconductor by the creation of acceptor levels in ZnO. However, doping with Group II elements like calcium is less studied. This element recently received more attention because of its important properties such as its non-

Corresponding Author: Ines Hajjej Mejri **Email**: ines.mejrihajjej24@gmail.com
Lassaad EL MIR **Email**: Lassaad.ElMir@fsg.rnu.tn

toxicity, abundance in nature, high chemical stability and low cost. Besides, it presents specific characteristics in the ZnO matrix which are very promising for several technological applications. Calcium can be used to enhance the particle size and optical properties of ZnO nanostructures. Although the ionic radius of Ca^{2+} (0.99 Å) is larger than that of Zn^{2+} (0.74 Å), we obtained a successful substitution of the Ca in the ZnO matrix. Further, to prepare the doped and undoped ZnO thin film, several physical and chemical techniques have been used, such as pulsed laser deposition (PLD) [19], RF magnetron sputtering [20], spray pyrolysis [21], sol-gel process [22], etc. As a versatile technique, the PLD is one of the most efficient methods. It is very unique and widely used for the growth of stoichiometric oxide thin film. It is relatively simple and offers more advantages compared to other physical vapour deposition methods. Mainly, the advantages of PLD techniques are the ability to create high-quality thin film fabricated at low temperatures. The deposition can be controlled by adjusting the pulse duration and the laser repetition rate [23]. Also, this method promotes the similarity of the composition of thin film to the target [24]. Therefore, many factors can influence the physical properties of doped and undoped ZnO thin film, such as substrate type, annealing temperature, oxygen pressure, and others [25-28]. Among these factors, we are interested in studying the effect of thickness. In reality, the latter has an effect on the size and the orientation of the crystallites and on the strains and lattice stresses of the studied material, which is linked to the optical and electrical properties. For this reason, several researchers are interested in studying this behaviour. Indeed, Mahdhi et al. [29] have reported the structural, electrical and optical properties of Ga-doped ZnO thin film with different thicknesses. Also, Pandey et al. [30] have studied the dependence of thickness on structural and optical properties of aluminium-doped zinc oxide thin film. Benramache et al. [31] focused on ZnO thin film deposited by ultrasonic sputtering.

This work aims to investigate the effect of thickness on structural and optical properties of Ca-doped ZnO thin film with an atomic concentration of 3% (CZO3%) from nanoparticles prepared by the sol-gel process. These films were deposited on glass substrates by the PLD technique with different thicknesses: 410, 480, 550, and 612 nm.

2. Experimental Details

Calcium-doped ZnO nanoparticles were synthesized via a sol-gel process using the autoclave system under supercritical conditions, following the protocol described by El Mir et al. [32, 33]. The precursors used are zinc acetate dihydrate [Zn $(CH_3COO)_2$. $2H_2O$] with purity higher than 99%, and as a doping element, an adequate quantity of calcium chloride hexahydrate [$CaCl_2$, $6H_2O$; 99%] which corresponds to [Ca/Zn] atomic ratio of 0.03. In the elaboration process, methanol and ethanol were used as solvents. The obtained nanopowder was deposited on a glass substrate by the pulsed laser deposition technique of the PLD/MBE 2100 type. Indeed, this powder was pressed inside the target holders of 2 inches in diameter under an axial pressure of 300 kg/cm^2 to obtain compact targets. Then it was sintered at 400°C for 2 hours in air. The laser (KrF excimer) was operated at a wavelength of 248 nm with a repetition rate of 10 Hz and a pulse width equal to 20 ns. This source was used, with an energy of 350 mJ to ablate the target. The growth pressure in the chamber was 10^{-6} Torr and the substrate temperature was 300°C. The chamber was filled with oxygen with a pressure of 5.10^{-3} Torr. The substrate was placed at 55 mm from the target. The growth parameters by PLD remain constant during the deposition time which is adjustable to have the different thicknesses (410, 480, 550, 612 nm). The structural properties of the synthesised samples were performed by X-ray diffraction spectrometer (*Bruker-D5005*) using a Cobalt K_α radiation (λ = 1.78901Å). The surface morphology of our thin film was observed using a scanning electron microscope (SEM, HITACHI S4500). The optical properties were investigated by a UV-Vis-IR spectrometer (Shimadzu UV-3101PC).

3. Results and Discussion

3.1. X-ray Diffraction

Figure 1 depicts the XRD patterns of the CZO thin film with different thicknesses (410, 480, 550, 612 nm). These diagrams reveal that all the samples have a hexagonal wurtzite structure of space group $P6_3mc$ with a preferential orientation (002) along the c-axis perpendicular to the substrate [34, 35]. The peak

position matches the standard JCPDS card No. 36-1451 [36]. Further, the absence of secondary phases indexed on the diagrams is noted, which indicates the good quality of the crystal structure of this thin film. It is also clear that there is an increase in the intensity of the (002) peak with the thickness, showing that the crystallinity of the thin film is improved [37, 38]. Indeed, the growth of these films is accompanied by the formation of nucleation centres and small crystallites. Thus, an improvement in crystallinity is observed as a result of increasing the thickness and the grain size. Besides, we focused on the peak (002) to present the offset of peak positions and the width at half maximum (FWHM). As seen in Fig. 2, the (002) peak shifts slightly toward higher diffraction angles with increasing thickness. This shift can be explained by residual stresses in the thin film due to a mismatch of the thermal expansion coefficient between the film and the glass substrate. We used the width at half maximum (FWHM) of the peak (002) to determine the crystallite size, the lattice parameter c, the strain, and the residual stresses of the CZO3% thin film from the following equations. The crystallite size was estimated using the Debye-Scherrer formula [39]:

$$D = \frac{K\lambda}{\beta \cos\theta} \quad (1)$$

where λ defines the X-ray wavelength (λ = 1.78901Å), θ is the diffraction angle, and β represents the full width at half maximum of the XRD peak.

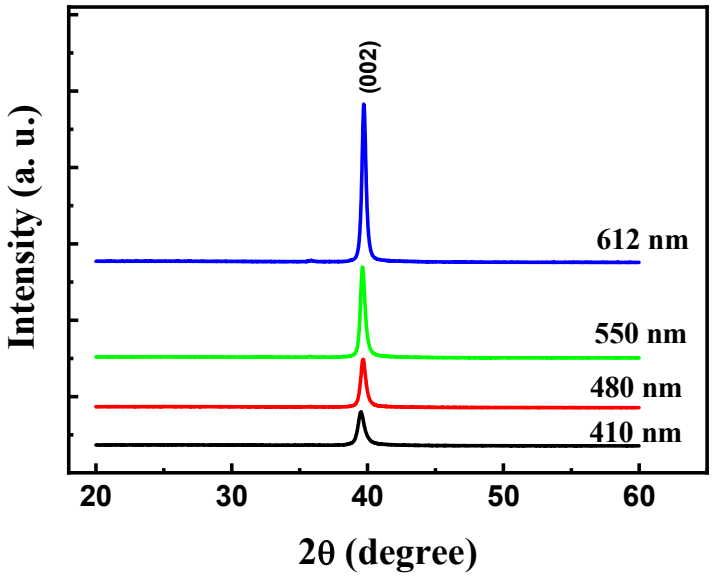

FIG. 1. XRD diagrams of CZO3% thin film with various thicknesses.

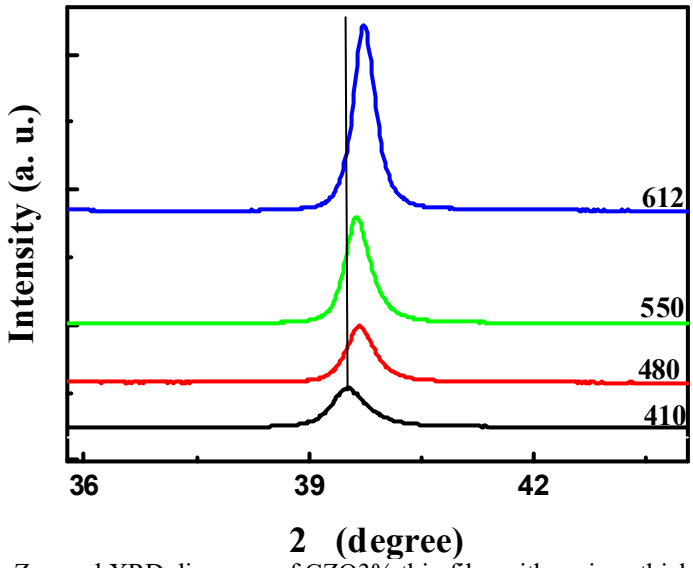

FIG. 2. Zoomed XRD diagrams of CZO3% thin film with various thicknesses.

The lattice parameter c for these films was calculated using the following formula [40]:

$$d = \frac{a}{\sqrt{\frac{4}{3}\left(h^2 + k^2 + hk\right) + l^2 \frac{a^2}{c^2}}} \quad (2)$$

where h, k, and l are the Miller indices, d_{hkl} is the interplanar spacing for (hkl), and a and c represent the lattice parameters. Subsequently, we used this parameter to determine the strain ε of the thin film using the Eq. (3) [41]:

$$\varepsilon\,(\%) = \frac{c - c_0}{c_0} \times 100 \quad (3)$$

where c is the lattice parameter of the strained films determined from XRD data and c_0 represents the unstrained lattice parameter of bulk ZnO (5.2065 Å) [42]. From the strain, we calculated the residual stress in the plane of the film using the following formula [43]:

$$\sigma = -233\ \varepsilon\ [GPa] \quad (4)$$

The obtained values are grouped in Table 1. From these values, we notice an increase in crystallite size D with thickness accompanied by a decrease of the width at half maximum β, which indicates the improvement in the crystallinity of the CZO thin film deposited on the glass substrate. Also, it is noted that the low elastic strain is for the highest thickness, which makes this film more relaxed and its crystallinity is enhanced. The residual stress also presents a very important parameter occurring during the deposition of thin film, which can be intrinsic or extrinsic [44]. In this study, we notice an increase in the residual stress σ(GPa) with increasing thickness and their values have a negative sign which proves that these films are in a state of compression. In addition, the lattice parameters (a, c) which were determined according to Bragg's law, decrease with increasing thickness. This result can be explained by a contraction in the crystal lattice. Also, the value of the parameter c for all the studied samples, is higher than those of ZnO without stress in the JCPDS card No. 5-664 (c_0 = 5.2065 Å) [32], justifying that these films undergo stress along the orientation of the c-axis in the presence of Ca.

TABLE 1. The crystallographic parameters of the CZO3% with various thicknesses

Thickness (nm)	410	480	550	612
$2\boldsymbol{\theta}$(°)	39.54	39.69	39.65	39.74
$\boldsymbol{\beta}$(°)	0.508	0.406	0.363	0.318
D (nm)	19	24	27	30
d_{hkl}(Å)	2.645	2.634	2.637	2.632
a (Å)	3.054	3.042	3.044	3.039
c (Å)	5.289	5.269	5.274	5.264
$\boldsymbol{\varepsilon}$ (%)	1.59	1.20	1.29	1.10
$\boldsymbol{\sigma}$ (GPa)	-3.68	-2.80	-3.01	-2.56

3.2. Morphological Analysis

The cross-sectional image and the surface morphology of the CZO thin film with a thickness of about 410 nm obtained by scanning electron microscopy are presented in Fig. 3(a) and 3(b). It is clear that this film has a uniform grain distribution with perpendicularly oriented columnar structure and the surface between the deposited film (CZO) and the substrate is well defined with low roughness, which indicates the good quality of the surface. The film presents a uniform grain size with a typical columnar structure and a smooth surface. The thickness of the film thickness agrees well with the optical study. The cross-section SEM image of the thin film indicates that it has a c-axis preferred orientation, due to the self-texturing mechanism as discussed by El Mir et al. [3], which concluded that film crystal orientation is a result of a self-ordering effect caused by the minimization of the crystal surface free energy as well as by the interaction between the deposited material and the substrate surface. Furthermore, according to the elemental analysis (Fig. 3(c)), all the desired elements are present and no impurities have been detected.

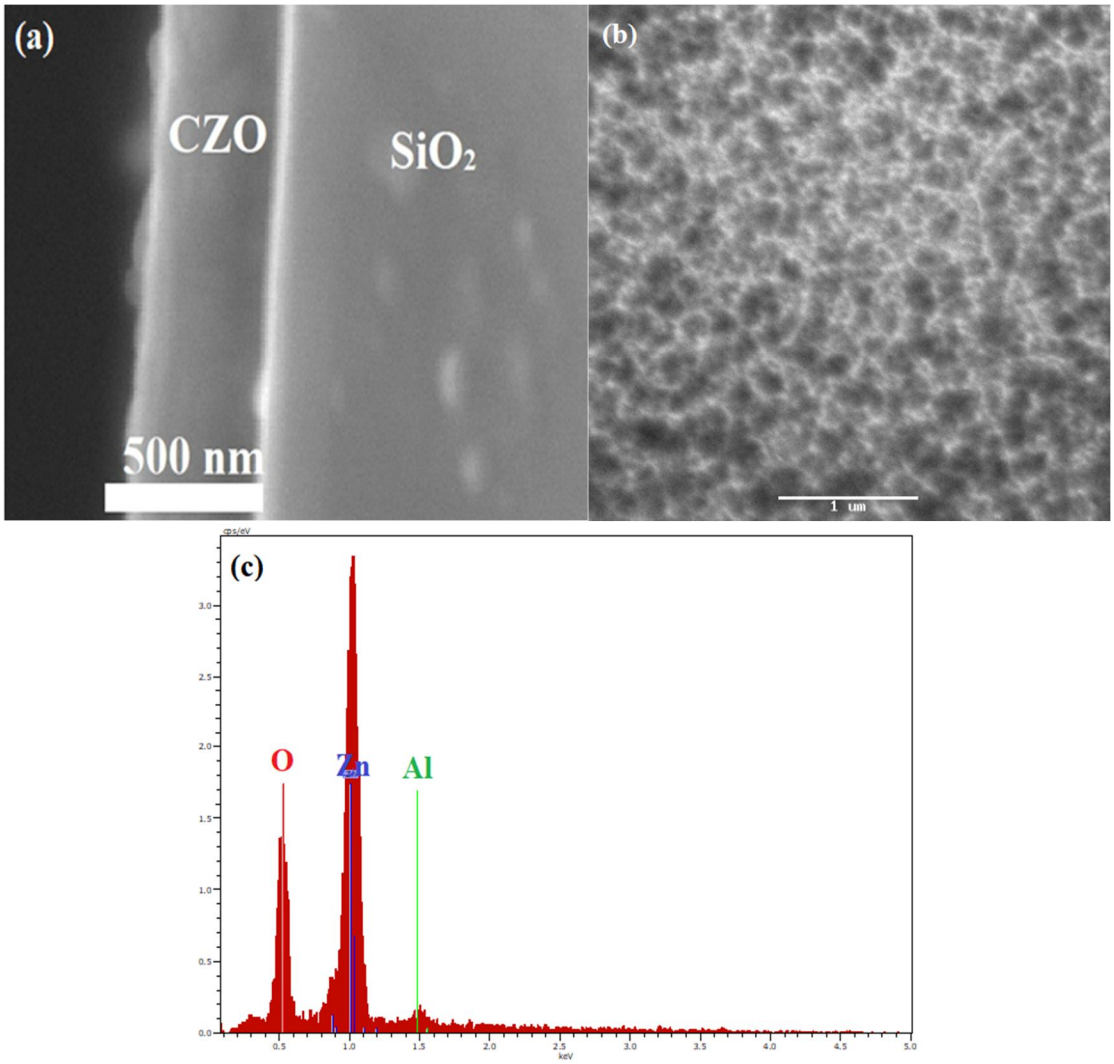

FIG. 3. (a) Cross-section SEM image, (b) SEM surface image, (c) EDX analysis of CZO3% thin film with a thickness of 410 nm.

3.4. Optical Properties

To study the effect of thickness on the optical properties of CZO thin film, the transmittance and absorbance for all samples were measured in the wavelength range between 200-2400 nm. These spectra are shown in Figs. 4 and 5. From these figures, we notice that all thin film samples exhibit high transparency in the visible and NIR regions and an important absorption in the UV region. As shown in Fig. 4, the average transmittance of all CZO3% thin film samples varies from 80% to 98% in the wavelength region above 400 nm, which indicates high transparency. This transparency depends on the thickness; the film with the lowest value (410 nm) corresponds to the highest transmittance. This is correlated to the increase in the concentration of charge carriers [45] and to the absorption of photons which is increasingly higher in the material as thickness increases. Further, we note the presence of interference fringes for all films, indicating their good quality and homogeneity [46] in addition to a less rough surface. This suggests that these films are suitable candidates for transparent electrodes for optoelectronic applications [47, 48]. Fig. 5 shows that in the wavelength region lower than 400 nm, the absorbance increases remarkably by increasing the thickness of our thin film. This high absorbance corresponds to a fundamental absorption in the films, which is due to the electronic transition from the valence band to the conduction band. This indicates the possibility of these films to serve as optical filters for ultraviolet rays and thus justifies the use of the absorption coefficient to determine the optical gap. The absorption coefficient (α) was calculated using the following equation [49]:

$$\alpha = \frac{1}{d}\ln\frac{1}{T} \quad (5)$$

where d is the thickness of the film and T is the transmittance. We then used this coefficient to determine the band gap energy E_g of our thin film following the Tauc relation [50]:

$$(\alpha h\upsilon)^2 = A(h\upsilon - E_g) \quad (6)$$

where A is the constant for direct transition and $h\upsilon$ is the photon energy. Fig. 6 displays the plot of $(\alpha h\upsilon)^2$ versus $(h\upsilon)$ for CZO thin film of different thicknesses. The optical band gap can be achieved by extrapolating the linear portion to the photon energy axis. The obtained values of the band gap energy for all samples are summarized in Table 2. From this table, we note a decrease of E_g as the thickness of the CZO thin film increases. This reduction may be due to the disorder caused by lattice defects in the material [51] and the change in crystallinity and strains in the films [52]. In fact, several factors can explain the variation in the gap energy and sometimes we have antagonistic behaviours. In our case, the decrease in the band gap energy can be mainly attributed to two effects: the first one is the increase in the concentration of defects which allows the increase in the width of the tail of the band. For the second effect, the quantum confinement, increasing the size makes it possible to reduce the energy of the gap, provided that the size is of the order of the Bohr radius of the material. Many authors have reported this same behaviour. For example, Udachan et al. [53] observed that the decrease of the band gap energy with increasing the thickness of selenium thin film is attributed to the nanocrystalline quantum size effect. Also, in the work of Bouderbala et al. [54] it was shown that the decrease of band gap energy with the increase of thickness of undoped ZnO thin film deposited by the rf-sputtering method is due to the carrier concentration variation. Furthermore, Revathi et al. [55] reported that the decrease in the optical band gap energy is attributed to the quantum confinement effect.

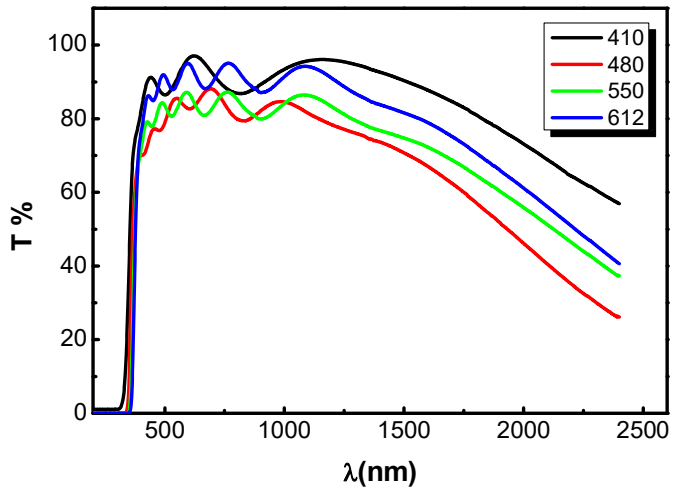

FIG. 4. Transmittance spectra of CZO3% thin film with various thicknesses (410, 480, 550, 612 nm).

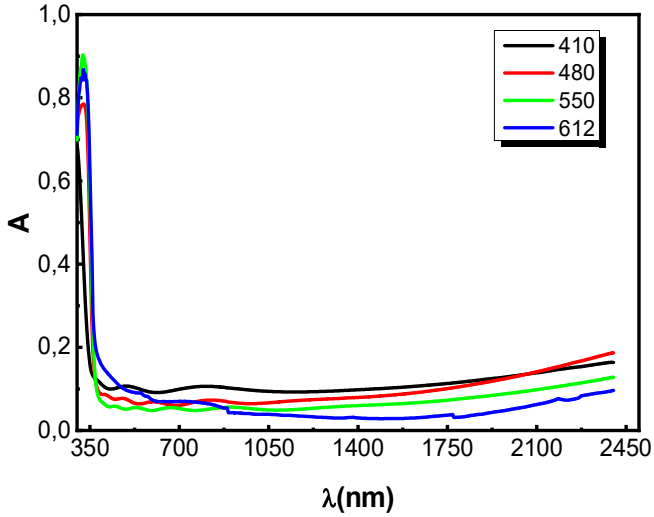

FIG. 5. Absorbance spectra of CZO3% thin film with various thicknesses (410, 480, 550, 612 nm).

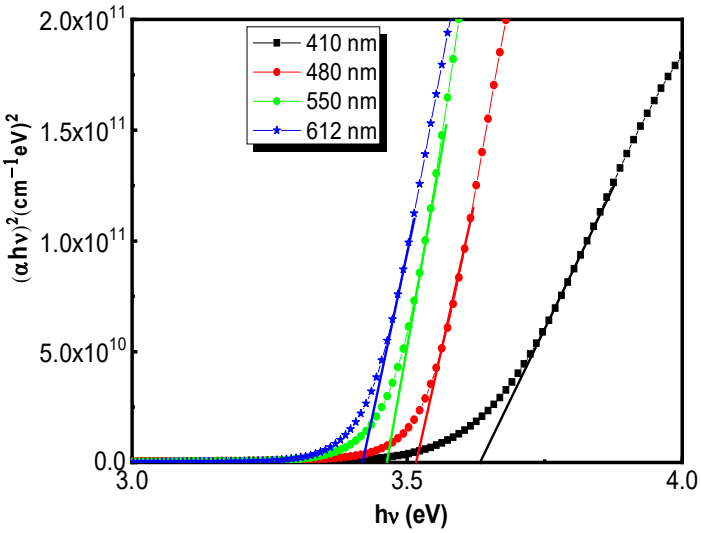

FIG. 6. Plots of $(\alpha h\upsilon)^2$ as a function of $(h\upsilon)$ of CZO3% thin film with different thicknesses.

TABLE 2. The optical band gap energy and Urbach energy of CZO3% with different thicknesses

Thickness (nm)	410	480	550	612
E_g (eV)	3.63	3.51	3.45	3.41
E_u (meV)	194.93	147.85	131.69	131.46

On the other hand, the Urbach energy E_u is a parameter that defines the purity and crystalline disorder in the material and provides information on the density of the energy states in the tail of the valence or conduction band. Following Urbach's Rule, the absorption coefficient is expressed by [56]:

$$\alpha = \alpha_0 \exp\left(\frac{h\upsilon}{E_u}\right) \quad (7)$$

Consequently, we can apply the following relation to plot $\ln(\alpha)$ as a function of $h\upsilon$:

$$\ln(\alpha) = \ln(\alpha_0) + \frac{h\upsilon}{E_u} \quad (8)$$

Thus, we can determine the value of the Urbach energy E_u from the inverse of the slope of the linear part of the traced curve (Fig. 7). The values obtained are summarized in Table 2. According to these results, we can see a reduction in the Urbach energy of our films as their thickness increases. This coincides with the improvement of the crystallinity of the CZO thin film and the increase in thickness which is proven by the XRD results. Generally, as the thickness of the ZnO thin film increases, the Urbach energy tends to decrease. This is often due to the reduction in the amount of surface and interface defects that induce localized energy levels in the band gap. The highest thickness can reduce the influence of these defects and improve the crystalline quality of the material, which results in a decrease in the Urbach energy. From the absorption coefficient, we can also determine the extinction coefficient k at different wavelengths λ. This coefficient presents the imaginary part of the complex refractive index, reflecting the absorption of radiation by the material. This parameter was determined using the following equation [57]:

$$k = \frac{\alpha\lambda}{4\pi} \quad (9)$$

Figure 8 shows that in the ultraviolet region, the value of the extinction coefficient is high for all samples. These large values are due to the intrinsic absorption of energies that are higher than the gap. We also notice a decrease in this coefficient with the wavelength reaching low values in the visible and infrared regions, which indicates the transparency of our films [58].

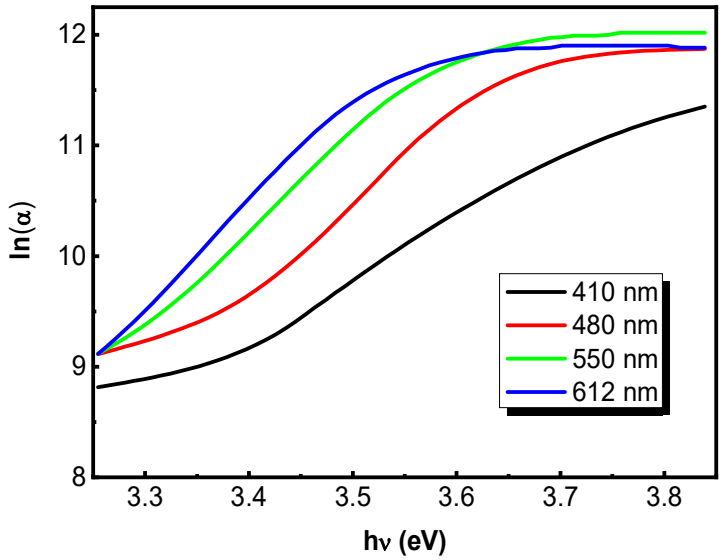

FIG. 7. Plot $\ln(\alpha)$ as a function of hυ of CZO3% with different thicknesses.

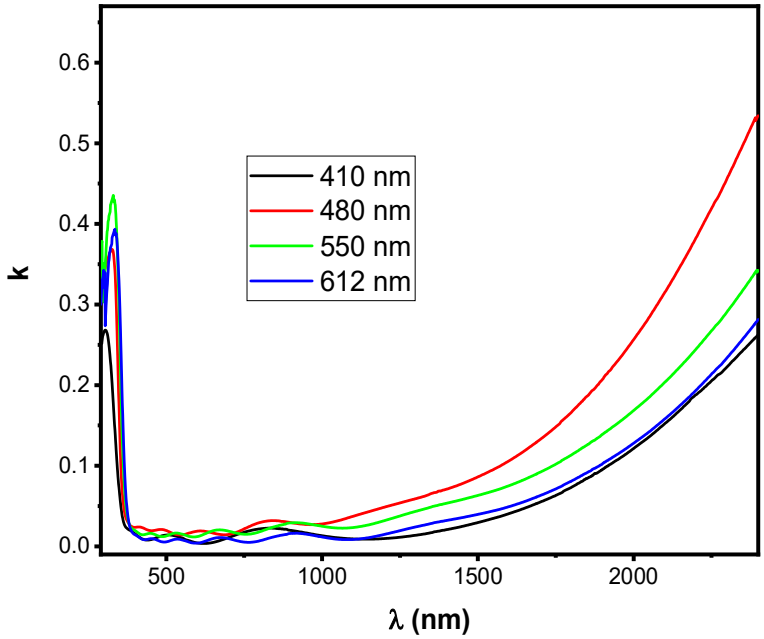

FIG. 8. Extinction coefficient as a function of wavelength of the CZO3% thin film at different thicknesses.

4. Conclusion

In summary, the effect of thickness on the structural and optical properties of thin film of CZO3% deposited by the PLD technique on the glass substrate based on nanoparticles doped and synthesised by the sol-gel technique was studied in detail. The structural analysis by X-ray diffraction showed that these films have a hexagonal wurtzite structure and a preferential orientation in (002) direction along the c-axis which is improved with the increase of thickness. Therefore, we proved that the crystallite size, the strains, the residual stresses, and lattice parameters depend on the thickness. It is evident that residual stresses have a significant effect on material properties; in particular, they can affect the band gap and thus influence all optical properties. For this reason, it is often necessary to select the right values for specific applications in optoelectronics. The results obtained by the optical study showed that these films are transparent in the visible-NIR region and the absorption is significant in the ultraviolet region. It was found that the band gap energy and the Urbach energy decreased with increasing thickness. The presented protocol implies that the laser ablation technique is promising for tailoring different properties of CZO thin film based on aerogel nanoparticles, producing high-quality TCO with tailored properties.

References

[1] Faramawy, A., Elsayed, H., Scian, C., and Mattei, G., Ceramics, 5 (2022) 1128.

[2] Omri, K., Najeh, I., and El Mir, L., Ceramics International, 42 (2016) 8940.

[3] El Mir, L., Ben Ayadi, Z., Saadoun, M., von Bardeleben, J., Djessas, K., and Zeinert, A., Physica Status Solidi A, 204 (2007) 3266.

[4] Zyoud, S.H., Alalamal, S.O., Hegazi, O.E., Yahia, I.S., Zahran, H.Y., Abu Sara, H., Haj Bloukh, S., Shahwan, M., Zyoud, A.H., Hassan, N., Ashames, A., Daher, M.G., Makhadmeh, G.N, Jairoun, A., Qamhieh, N., and Abdelwahab, M.Sh, Journal of Catalysis, 13 (2023) 900.

[5] Zyoud, S.H., Abdullah, C.A.C., Ashames, A., Hassan, N., Yahia, I.S., Zyoud, A.H., Zahran, H.Y., Qamhieh, N., Makhadmeh, G.N., and AlZoubi, T., Results in Engineering, 24 (2024) 102875.

[6] Zyoud, S.H., Ashames, A., Zyoud, A.H., Prasad, A.R., Abdullah, C.A.C., Zyoud, S.H., Yahia, I.S., Makhadmeh, G.N, Khalid, A., Qamhieh, N., Zahran, H.Y., Muhammad, S., and Abdelwahab, M.Sh., Materials Science and Engineering B, 30 (2024) 117649.

[7] Hjiri, M., Aida, M.S., Lemine, O.M., and El Mir, L., Materials Science in Semiconductor Processing, 89 (2019) 149.

[8] El Ghoul, J., Omri, K., El Mir, L., Barthou, C., and Alaya, S., Journal of Luminescence, 132 (2012) 2288.

[9] Salma, R., Ghribi, F., Houas, A., Barthou, C., and El Mir, L., International Journal of Nanoelectronics and Materials, 3 (2010) 133.

[10] Zyoud, S.H., AlRadi, B.M., AlMaamari, B.M., Nasor, Zahran, H.Y., Yahia, I.S., Ahmad, T., Khan, S.N., Zyoud, A.H., Shahwan, M., Hassan, N., Ashames, A., Daher, M.G., Makhadmeh, G.N., Qamhieh, N., Jairoun, A.A., and Abdelwahab, M.Sh., Indian Journal of Physics, 98 (2024) 54.

[11] Zyoud, S.H., Hegazi, O.E., Alalamal, S.O., Yahia, I.S., Zahran, H.Y., Haj Bloukh, S., Abu Sara, H., Zyoud, A.H., Shahwan, M., Ashames, A., Hassan, N., Daher, M.G., Makhadmeh, G.N., Jairoun, A.A., and Kamoun, E.A., Applied Physics A, 129 (2023) 750.

[12] Erouel, M., Mansouri, S., Ba, M., Romero, A., Jiménez-Tejada, J.A., and El Mir, L., Journal of Electronic Materials, 52 (2023) 5315.

[13] Rana, V.S., Rajput, J.K., Pathak, T.K., and Purohit, L.P., Journal of Alloys and Compounds, 764 (2018) 724.

[14] Tiwari, A. and Sahay, P.P., Brazilian Journal of Physics, 52 (2022) 176.

[15] Mourad, S., ElGhoul, J., Khettou, A., Mari, B., AbdelAll, N., Khouqeer, G., El Mir, L., and Khirouni, K., Physica B: Condensed Matter, 626 (2022) 413577.

[16] Ouarez, L., Chelouche, A., Touam, T., Mahiou, R., Djouadi, D., and Potdevin, A., Journal of Luminescence, 203 (2018) 222.

[17] Khlifi, N., Ihzaz, N., Toulemande, O., Dandre, A., Labrugère-Sarroste, C., Bessadok, M.N., Lemine, O.M., and El Mir, L., RSC Advances, 14 (2024) 27622.

[18] Liu, L., Bao, Q., Zhao, T., Liu, K., Shi, D., Li, S., Zhu, W., Li, X., and Zhou, J., Modern Physics Letters B, 38 (2024) 2450213.

[19] Alyamani, A., Tataroğlu, A., El Mir, L., Al-Ghamdi, A.A., Dahman, H., and Farooq, W.A., Applied Physics A, 122 (2016) 1.

[20] Khalfallah, B., Riahi, I., and Chaabouni, F., Optical and Quantum Electronics, 53 (2021) 238.

[21] Kurtaran, S., Optical Materials, 114 (2021) 110908.

[22] Mejri, I.H., Omri, K., Mrabet, S., Moutia, N., Gouadria, S., and El Mir, L., Journal of Materials Science: Materials in Electronics, 33 (2022) 6485.

[23] Zhao, L., Lian, J., Liu, Y., and Jiang, Q., Applied Surface Science, 252 (2006) 8451.

[24] Wei, X.Q., Huanga, J.Z., Zhanga, M.Y., Dua, Y., and Manb, B.Y., Materials Science and Engineering B, 166 (2010) 141.

[25] Yang, J., Lang, J., Li, C., Yang, L., Han, Q., Zhang, Y., Wang, D., Gao, M., and Liu, X., Applied Surface Science, 255 (2008) 2500.

[26] Zak, A.K., Abrishami, M.E., Majid, W.H.A., Yousefi, R., and Hosseini, S.M., Ceramics International, 37 (2011) 393.

[27] Zhaoyang, W. and Lizhong, H., Vacuum, 83 (2009) 906.

[28] Rahmane, S., Aida, M.S., Djouadi, M.A., and Barreau, N., Superlattices and Microstructures, 79 (2015) 148.

[29] Mahdhi, H., Alaya, S., Gauffier, J.L., Djessas, K., and Ayadi, Z.B., Journal of Alloys and Compounds, 695 (2017) 697.

[30] Pandey, R.K., Ghosh, K., Mishra, S., Bange, J.P., Bajpai, P.K., and Gautam, D.K., Materials Research Express, 5 (2018) 086408.

[31] Benramache, S., Aoun, Y., Lakel, S., and Benhaoua, B., Materials Research Express, 12 (2019) 126418.

[32] El Mir, L. and Omri, K., Superlattices and Microstructures, 75 (2014) 89.

[33] El Mir, L., Amlouk, A., Barthou, C., and Alaya, S., Physica B: Condensed Matter, 388 (2007) 412.

[34] Sui, Y.R., Yao, B., Yang, J.H., Cui, H.F., Huang, X.M., Yang, T., Gao, L.L., Deng, R., and Shen, D.Z., Applied Surface Science, 256 (2010) 256.

[35] Ellmer, K., Cebulla, R., and Wendt, R., Thin Solid Films, 317 (1998) 413.

[36] Ben Ayadi, Z., Mahdhi, H., Djessas, K., Gauffier, J.L., El Mir, L., Alaya, S., Thin Solid Films, 553 (2014) 123.

[37] Ameur, S.B., Barhoumi, A., Belhadj-ltaief, H., Mimouni, R., Duponchel, B., Leroy, G., Amlouk, M., and Guermazi, H., Materials Science in Semiconductor Processing, 61 (2017) 17.

[38] Samavati, A., Nur, H., Ismail, A.F., and Othaman, Z., Journal of Alloys and Compounds, 671 (2016) 170.

[39] Scherrer, P., Mathematisch-Physikalische Klasse, 1918 (1918) 98.

[40] Peng, L.P., Fang, L., Yang, X.F., Li, Y.J., Huang, Q.L., Wu, F., and Kong, C.Y., Journal of Alloys and Compounds, 484 (2009) 575.

[41] Ong, H.C., Zhu, A.X.E., and Du, G.T., Applied Physics Letters, 80 (2002) 941.

[42] Cullity, B.D., "Elements of X-ray Diffraction", (Addison Wesley Publishing Company, 1978).

[43] Shashikant, S., Periasamy, C., and Chakrabarti, P., Electronic Materials Letters, 11 (2015) 1093.

[44] El Mir, L., Journal of Inorganic and Organometallic Polymers and Materials, 31 (2021) 2648.

[45] Coutts, T.J., Young, D.L., and Li, X., MRS Bulletin, 25 (2000) 58.

[46] Ilican, S., Caglar, M., and Caglar, Y., Material Sciences-Poland, 25 (2007) 709.

[47] El Mir, L., Journal of Luminescence, 186 (2017) 98.

[48] Yanfeng, S., Liu, W., Zhidan, H., Shaolin, L., Yi, Z.Z., and Du, G., Vacuum, 80 (2006) 981.

[49] Huang, C.J., Meen, T.H., Lai, M.Y., and Chen, W.R., Solar Energy Materials & Solar Cells, 82 (2004) 553.

[50] Tauc, J., Materials Research Bulletin, 3 (1968) 37.

[51] Mortezaali, A., Taheri, O., and Hosseini, Z.S., Microelectronic Engineering, 151 (2016) 19.

[52] Shim, E.S., Kang, H.S., Kang, J.S., Kim, J.H., and Lee, S.Y., Applied Surface Science, 186 (2002) 474.

[53] Udachan, S., Ayachit, N., Udachan, L., and Halembre, R., Ing. Univ., 25 (2021) 2.

[54] Bouderbala, M., Hamzaoui, S., Amrani, B., Reshak, A.H., Adnane, M., Sahraoui, T., and Zerdali, M., Physics B, 403 (2008) 3326.

[55] Revathi, R., Revathi, S., Jothiramalingam, R., Sukumar, M., Basith, N.M., Sundararajan, M., Yuvaraj, S., and Arokiyraj, S., Digest Journal of Nanomaterials and Biostructures, 18 (2023) 1587.

[56] Badreddine, K., Kazah, I., Rekaby, M., and Awad, R., Journal of Nanomaterials, 2018 (2018) 1.

[57] Manifacier, J.C., Gasio, J., and Fillard, J.P., Journal of Physics E: Scientific Instruments, 9 (1976) 1002.

[58] Xue, S.W., Zu, X.T., Zhou, W.L., Deng, H.X., Xiang, X., Zhang, L., and Deng, H., Journal of Alloys and Compounds, 448 (2008) 21.